CHEMISTRY
A EUROPEAN JOURNAL

DOI: 10.1002/chem.200601143

Selective Chemisorption of Carbon Monoxide by Organic–Inorganic Hybrid Materials Incorporating Cobalt(III) Corroles as Sensing Components

Jean-Michel Barbe,* Gabriel Canard, Stéphane Brandès, and Roger Guilard*[a]

Abstract: Twenty-one hybrid materials incorporating cobalt(III) corrole complexes were synthesized by a sol–gel process or by grafting the metallocorrole onto a mesostructured silica of the SBA-15 type. All the materials show an almost infinite selectivity for carbon monoxide with respect to dinitrogen and dioxygen in the low-pressure domain where the chemisorption phenomenon is predominant. This peculiar property is of prime importance for an application as a CO sensor. The selectivity slightly decreases at high pressures where nonselective physisorption phenomena mainly occur. The percentage of active sites for CO chemisorption ranges from 22 to 64%. This low percentage may be attributable to interactions between the cobalt(III) corroles with silanol or siloxane groups remaining at the surface of the materials which prevent further coordination of the CO molecule. Notably, the most efficient materials are those prepared in the presence of a protecting ligand (pyridine) during the gelation or the grafting process. The removal of this ligand after the gelation process releases a cavity around the cobalt ion that favors the coordination of a carbon monoxide molecule. The CO adsorption properties of the SBA-15 hybrid were not affected over a period of several months thus indicating a high stability of the material. Conversely, the xerogel capacities slowly decrease owing to the evolution of the material structure.

Keywords: CO detection · cobalt · corroles · organic–inorganic hybrid composites · sol–gel processes

Introduction

Since the pioneering work of Johnson and co-workers in 1964, corrole chemistry has experienced a nearly exponential growth.[1–3] Initially, only β-pyrrole-substituted corrole macrocycles were available;[4] however, more recently, *meso*-substituted compounds have been synthesized in one or two steps to afford gram quantities of these derivatives.[5–12] Interesting applications of metallocorroles have already been reported in various fields, such as catalysis,[13–18] enzyme modeling[19] and gas sensing.[20,21] Our activities focus on the latter application field.

In a previous paper, we demonstrated that cobalt(III) corroles exhibited an infinite selectivity for carbon monoxide with respect to N_2 and O_2.[20] This peculiar property, which enables their use as sensing components for gas detectors, resulted from the selective coordination of CO to the central Co^{III} ion by a chemisorption process, whereas N_2 and O_2 could not coordinate. Moreover, we also showed that the reversibility of the CO adsorption at room temperature by cobalt(III) corroles strongly depends on the electronic properties of the substituents located at the periphery of the corrole macroring, that is, the affinity for CO increases with an increasing electron-withdrawing effect of the substituents and therefore with the Lewis acid character of the Co^{III} ion while the reversibility of the adsorption decreases concomitantly.[20]

More recently, in a preliminary report, we used the sol–gel process to immobilize corrole macrocycles in a silica matrix by means of one Si–C covalent bond.[21] The sol–gel chemistry allows the preparation of hybrid organic-inorganic materials, so-called polysilsesquioxanes[22–24] in which the organic units are located within the inorganic framework. Most often, the gelation of the polyalkoxysilane precursors leads to a nano-organization of the molecular units over a short[25,26] or a long range.[27,28] This nano-organization depends on the reaction conditions and the ability of the precursors to self-assemble by means of hydrogen bonds and

[a] Dr. J.-M. Barbe, Dr. G. Canard, Dr. S. Brandès, Prof. Dr. R. Guilard
Laboratoire d'Ingénierie Moléculaire pour la Séparation et les Applications des Gaz (LIMSAG, CNRS UMR 5633)
Université de Bourgogne, UFR Sciences et Techniques
9 avenue Alain Savary, BP 47870, 21078 Dijon Cedex (France)
Fax: (+33) 380-396-117
E-mail: Jean-Michel.Barbe@u-bourgogne.fr
Roger.Guilard@u-bourgogne.fr

Supporting information for this article is available on the WWW under http://www.chemeurj.org/ or from the author.

van der Waals interactions. We have shown that the Co^{III} metallocorrole-functionalized materials still exhibited a very high selectivity for CO binding in the low-pressure domain, concomitantly with an increased stability of the Co^{III} corrole complex incorporated in the material with respect to the isolated species.[21] This synthetic process is suitable for the preparation of thin films coated on a solid support, which greatly facilitates the elaboration of a gas sensor with a long-term stability. The materials prepared in the former study were obtained from the copolycondensation of corroles, monofunctionalized by a chain bearing a reactive trialkoxysilyl terminal group, with tetraethoxysilane (TEOS) or methyltriethoxysilane (MTEOS) under typical sol–gel reaction conditions.[21] Several corrole macrocycles bearing one, two, or three reactive trialkoxysilyl terminal groups were also synthesized and physicochemically characterized[29] to be used as precursors of organic-inorganic hybrid materials and to study the influence of the number of polycondensation directions on the reactivity and accessibility of the metallocorrole towards carbon monoxide binding.

Herein we describe the synthesis, physicochemical characterization, and adsorption properties of new organic–inorganic sol–gel materials incorporating these latter mono-, di- and trifunctionalized corrole macrocycles.

Ordered mesoporous silicas provide a rigid and uniform open-pore structure in contrast to sol–gel materials, which exhibit small pore sizes, a non-open-pore structure as well as a lack of mesoporous size control. Mesoporous silicas with uniform large channels and a stable two-dimensional hexagonal[30–32] (SBA-15), cubic[33] (SBA-16), or wormlike[34] (HMS, MSU) structure have already been described. To further study the influence of the inorganic matrix on the adsorption properties of the metallocorrole materials, an ordered mesoporous silica of the SBA-15 type was functionalized into the pores by grafting on the silanol functions the mono- and difunctionalized corrole in such a way to ensure easy access to the active sites. The synthesis of the SBA-15 silica starts from the Pluronic nonionic triblock copolymer as a structure-directing agent. This allows fine-tuning of the porous structure over a wide range of pore sizes (50–300 Å) depending on the reaction conditions, namely, temperature, ionic strength, and use of a swelling agent (decane, mesitylene). The striking features of the SBA-15 mesoporous silica are the narrow pore size distribution and high specific surface area (500–1000 $m^2 g^{-1}$), which enable a high functionalization rate. The synthesis and physicochemical characterization of SBA-15-type materials are also described in the present study.

Results and Discussion

Three types of differently substituted corrole macrocycles were used as precursors of organic-inorganic hybrid materials, depending upon the number of triethoxysilyl terminal groups. Mono- (M derivatives), di- (D derivatives) and trifunctionalized (T derivatives) corrole macrocycles have already been synthesized and physicochemically characterized.[29] The metalation of the free-bases was carried out under classical conditions using cobalt(II) acetylacetonate in a dichloromethane/ethanol mixture. Main spectroscopic features of these derivatives are summarized in the Experimental Section. The structures of all the synthesized cobalt(III) complexes are given in Scheme 1.

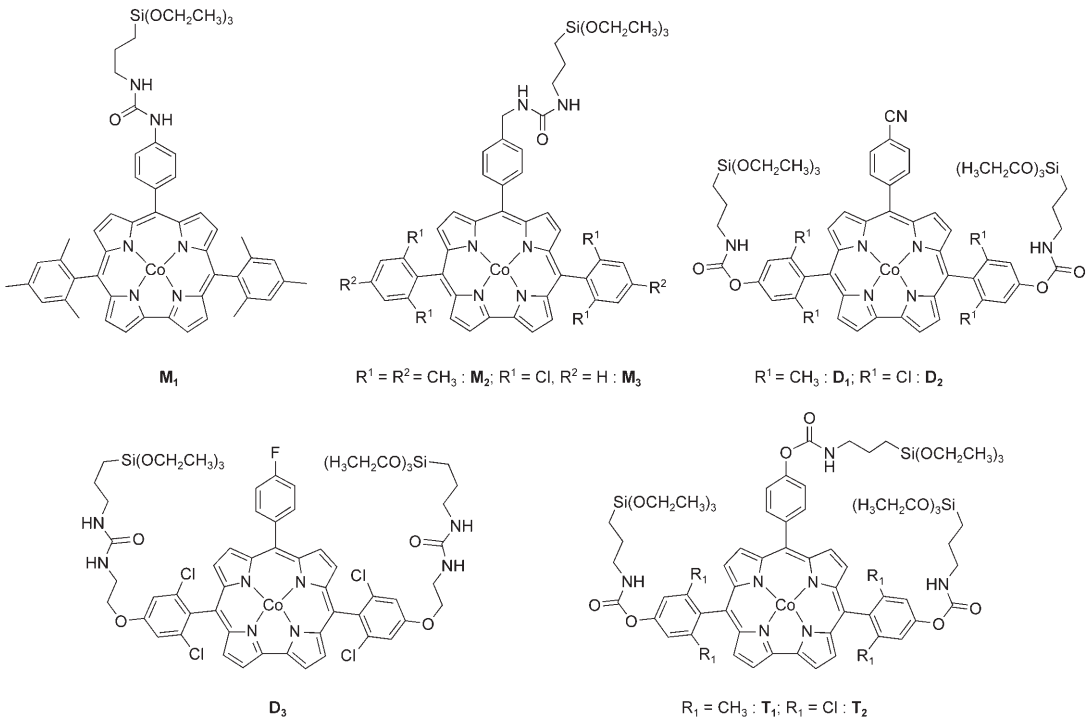

Scheme 1. Structures of the material precursors (M stands for mono-, D for di-, and T for trifunctionalized complex).

Different hybrid materials were prepared depending on the nature of the complex and the cogelation agent, the presence of a protecting ligand during the gelation process, and the reaction conditions. To visualize all these different parameters, a dedicated formulation is proposed in Scheme 2 for the hybrid materials. A similar formulation is used for the materials obtained by grafting corroles onto the mesostructured SBA-15 silica (see below).

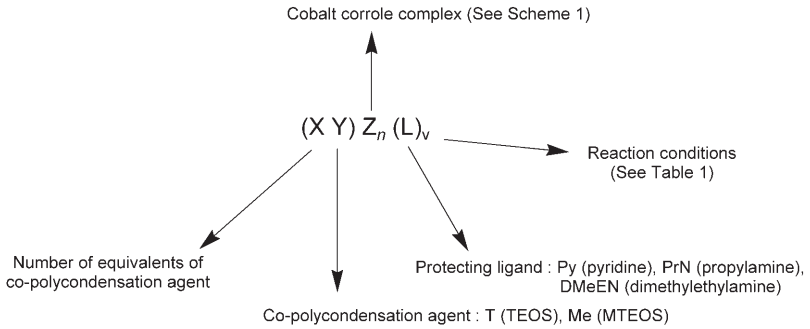

Scheme 2. Formulation used for the cogels incorporating Co^{III} corroles. Example: **(40T)D$_1$(PrN)$_A$**: $X=40$, Y = T (TEOS), $Z_n=D_1$(difunctionalized complex 1), L = PrN (propylamine), v = A (conditions A given in Table 1).

Incorporation of cobalt(III) corroles into hybrid materials by means of the sol–gel process

Monofunctionalized complexes: In the first step, as described in our preliminary report, we prepared the **(40T)M$_{1A}$** material from the co-polycondensation reaction of **M$_1$** (Scheme 1) with 40 equivalents of tetraethoxysilane (TEOS), in a stoichiometric amount of distilled water in THF as the solvent in the presence of tetrabutylammonium fluoride (TBAF, 1 mol% with respect to silicon) as a catalyst (conditions A given in Table 1).[21] Gelation was carried out at room temperature, and led to a xerogel after a 7 day aging period (Scheme 3). For the sake of comparison and in strictly identical experimental conditions, a hybrid material was synthesized from the free base corresponding to **M$_1$**.[21] The addition of pyridine during the gelation of **M$_1$** led to the formation of **(40T)M$_1$(Py)$_A$** under conditions A (see Table 1 and Scheme 3). Different experimental conditions were necessary (conditions B in Table 1) in order to initiate the co-polycondensation of methyltriethoxysilane (MTEOS) with **M$_1$** leading to **(40Me)M$_1$(Py)$_B$**, namely, 40 equivalents of MTEOS, distilled water, excess Py, and TBAF (5 mol%) (Scheme 3).[21] Pyridine was added during the gelation process to avoid the coordination of the free silanol and siloxane groups of the inorganic part to the cobalt(III) ions thus keeping the cobalt axial coordination site free for subsequent CO binding. Py was tentatively removed from the **(40T)M$_1$(Py)$_A$** and **(40Me)M$_1$(Py)$_B$** materials by a simple treatment under vacuum at room temperature. The absence of any Py molecule on **(40T)M$_1$(Py)$_A$** was clearly evidenced by comparison of the solid-state UV-visible spectra of **(40T)M$_{1A}$** and **(40T)M$_1$(Py)$_A$** which exhibited a single Soret band at 400 nm and broad Q bands (500–650 nm). In contrast, for **(40Me)M$_1$(Py)$_B$** the presence of a band at about 620 nm indicated that there were still two pyridine molecules on the cobalt ion.[35] Therefore, a higher temperature (200 °C) and a vacuum (10^{-3} Torr) were needed to fully eliminate pyridine from **(40Me)M$_1$(Py)$_B$**. Further characterization of the materials by ^{29}Si CP/MAS NMR indicated a high level of condensation for these hybrids.[21] To obtain more porous materials, co-hydrolysis was carried out in hot pyridine (conditions C) using **M$_2$** and MTEOS as the co-polycondensation agent (See Table 1 and Scheme 3). After three days, the resulting **(40Me)M$_2$(Py)$_C$** was thoroughly washed with methanol and dried under vacuum to remove any trace of remaining pyridine. Solid-state UV-visible data were in accordance with the absence of Py coordinated to the cobalt corrole complex, and ^{29}Si CP/MAS NMR data clearly showed the presence of the T^3 [C-*Si*(OSi)$_3$] substructure as well the absence of Q^3 [*Si*(OSi)$_3$(OR)] and Q^4 [*Si*-(OSi)$_4$] subunits,[36] thus indicating that no Si–C bond cleavage occurred during the polycondensation process at the higher temperature.

Table 1. Texture characteristics of the xerogels.

	Material[a]	S_{BET}[b] [m^2g^{-1}]	V_t[b] [cm^3g^{-1}]	V_m[b] [cm^3g^{-1}]
1	**(40T)M$_{1A}$**[c]	517	0.61	0.14
2	**(40T)M$_1$(Py)$_A$**[c]	418	0.75	0.09
3	**(40Me)M$_1$(Py)$_B$**[c]	12	0.03	–
4	**(40Me)M$_2$(Py)$_C$**	523	0.89	0.05
5	**(40T)D$_1$(Py)$_A$**	514	1.39	0.07
6	**(60T)D$_1$(Py)$_A$**	563	0.79	0.14
7	**(80T)D$_1$(Py)$_A$**	510	0.65	0.14
8	**(100T)D$_1$(Py)$_A$**	556	0.47	0.17
9	**(40T)D$_1$(PrN)$_A$**	310	0.79	0.04
10	**(40T)D$_2$(Py)$_B$**	363	0.53	0.08
11	**(40T)D$_2$(PrN)$_A$**	356	0.28	0.12
12	**(40T)D$_3$(Py)$_A$**	420	0.90	0.07
13	**(40T)T$_1$(Py)$_B$**	474	0.87	0.06
14	**(40T)T$_1$(DMeEN)$_B$**	431	0.93	0.03
15	**(40T)T$_2$(Py)$_B$**	373	0.42	0.08

[a] Conditions: A) THF, 25 °C, 1% TBAF; B) THF, 25 °C, 5% TBAF; C) Py, 110 °C, 5% TBAF. [b] S_{BET}: specific surface area; V_t: total pore volume; V_m: micropore volume; pore diameter $10<\varnothing<1000$ Å. [c] From ref. [21].

Difunctionalized complexes: Metallocorroles with two polycondensation directions were also studied. Complexes **D$_1$**, **D$_2$**, and **D$_3$**, bearing two triethoxysilyl-functionalized arms anchored to the macroring, were used to prepare the hybrid materials (See Scheme 1 for the structure of the complexes). **D$_1$** and **D$_2$** complexes differ by the presence of methyl groups (**D$_1$**) or Cl atoms (**D$_2$**) at the *ortho* positions of the

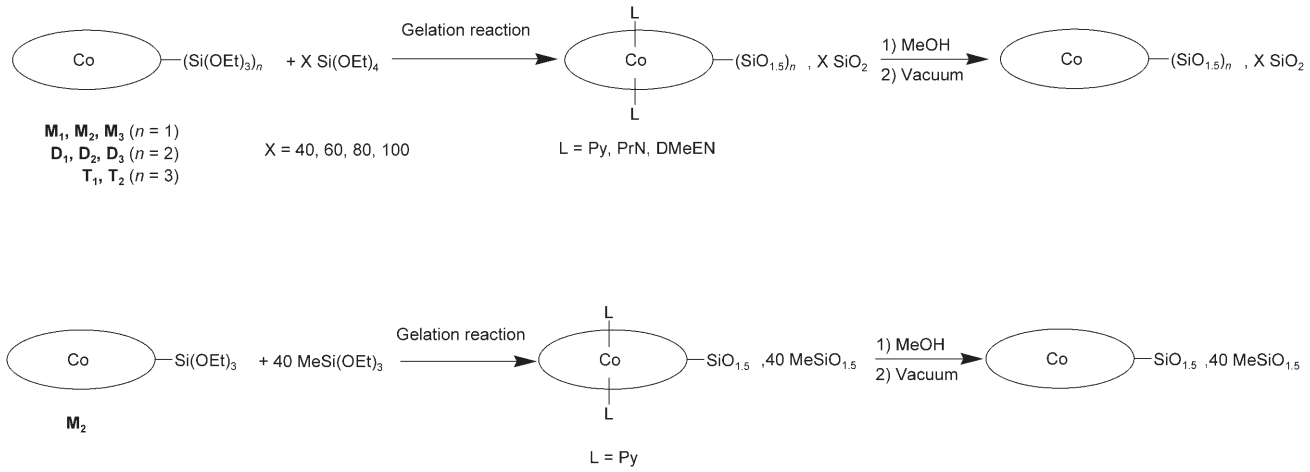

Scheme 3. Reaction scheme to synthesize metallocorrole-functionalized xerogels.

meso-phenyl rings; the Lewis acid character of the central cobalt metal is therefore enhanced in $\mathbf{D_2}$ compared to $\mathbf{D_1}$ (Scheme 1). Four hybrids were obtained from complex $\mathbf{D_1}$ by varying the amount of TEOS (40, 60, 80, and 100 equiv) in conditions A with pyridine to complete the coordination sphere of the Co^{III} ion (Table 1). This experiment was carried out to evaluate the influence of the dilution of the active Co^{III} complex inside the inorganic matrix on the reactivity of the materials towards CO. Similarly, one organic–inorganic material was obtained from $\mathbf{D_1}$ in conditions A in the presence of 40 equivalents of TEOS and excess propylamine (PrN) as the axial ligand (instead of Py) during the gelation process (Table 1). Conditions A were inappropriate to synthesize a material from $\mathbf{D_2}$ if pyridine was used as the axial ligand, and 5 mol% TBAF was required (conditions B in Table 1). Conversely, conditions A were sufficient with PrN as the ligand and the $\mathbf{D_2}$ complex. Finally, variation of the length of the chain bearing the triethoxysilyl function was investigated. Therefore, a material incorporating the $\mathbf{D_3}$ complex was synthesized (Scheme 1) using conditions A to initiate the gelation process. A total of eight organic–inorganic hybrid materials were obtained from difunctionalized complexes $\mathbf{D_1}$, $\mathbf{D_2}$, and $\mathbf{D_3}$ (see Scheme 2 and Scheme 3). As described for monofunctionalized complexes, all hybrids were washed with methanol and dried under vacuum. TGA/MS and UV/Vis data confirmed the absence of a coordinated molecule (Py or PrN) on the central cobalt(III) ion after the latter treatment (see the Experimental Section for a summary of the data).

Trifunctionalized complexes: Hybrid materials incorporating the trifunctionalized complexes $\mathbf{T_1}$ and $\mathbf{T_2}$ were also prepared (Scheme 1). Owing to the presence of different groups at the *ortho* positions of the *meso*-phenyl rings of the corrole (Cl or CH_3), these two latter complexes, similar to complexes $\mathbf{D_1}$ and $\mathbf{D_2}$, induce a different Lewis acid character for the central cobalt atom (Lewis acid character of the Co^{III} ion being superior in $\mathbf{T_2}$ compared to $\mathbf{T_1}$). Three xerogels were synthesized by co-polycondensation of $\mathbf{T_1}$ or $\mathbf{T_2}$ in the presence of 40 equivalents of TEOS, a stoichiometric amount of water, a catalytic amount of TBAF (5 mol% with respect to silicon) in THF at room temperature (conditions B in Table 1). The gelation reaction was performed in the presence of excess pyridine or *N,N′*-dimethylethylamine (DMeEN) with respect to the cobalt corrole complex. The gels were aged for one week, washed several times with methanol, and dried under vacuum. The absence of Py or DMeEN on the corrole cobalt ion was demonstrated by TGA/MS and UV/Vis measurements (see the Experimental Section for data).

Textural characterization of the hybrid materials: The specific surface area and pore diameters were determined from nitrogen adsorption experiments and calculated from BET[37] and BJH[38] analyses. Data are gathered in Table 1. Almost all the materials exhibit a large specific surface area and pore size distribution. Pores include micropores ($0 < \varnothing < 20$ Å), mesopores ($20 < \varnothing < 500$ Å) and few macropores ($500 < \varnothing < 1000$ Å). The only exception is the $\mathbf{(40Me)M_1(Py)_B}$ xerogel (Table 1, entry 3), prepared by co-polycondensation with MTEOS, which is almost nonporous ($12\ m^2 g^{-1}$). This low value results from the preparation of the material at 25 °C. Indeed, when the temperature is increased to 110 °C in pyridine (conditions C), the specific surface area concomitantly increases to $\approx 500\ m^2 g^{-1}$. This is the case for $\mathbf{(40Me)M_2(Py)_C}$ hybrid material, which exhibits a S_{BET} equal to $523\ m^2 g^{-1}$ (Table 1, entry 4). On the other hand, dilution in the silica matrix by co-hydrolysis with TEOS of the $\mathbf{D_1}$ metallocorrole possessing two polycondensation directions has little effect on the specific surface area; however, it does lead to a decrease in the total pore volume (V_t) while micropore volume (V_m) increases slightly (Table 1, entries 5–8). The hybrids prepared with propylamine as a protecting ligand are less porous than those synthesized with Py (entries 5 and 9, Table 1). Finally, using the same conditions, the total pore volume decreases as the length of the functionalized chain increases (Table 1, entries 5 and 12).

Gas adsorption measurements: CO, O_2, and N_2 adsorption measurements were carried out for all the described xerogels, including that obtained from the free base corresponding to $\mathbf{M_1}$. CO adsorption data are summarized in Table 2, while data relative to O_2 and N_2 adsorption are given in Table S1.

The gas volumes (CO, O_2, and N_2) adsorbed by the free-base material were very low and resulted from physisorption of the gases on the solid. The preliminary reported experiments provided clear evidence that O_2 and N_2 adsorption by **(40T)M$_{1A}$**, **(40T)M$_1$(Py)$_A$**, and **(40Me)M$_1$(Py)$_B$** materials also involves physisorption processes, whereas a chemisorption process explains the high affinity for CO. Very high CO/O_2 and CO/N_2 selectivities were determined from the adsorption measurements, which argued for CO detection purposes in an ambient atmosphere.[21] This data results from the selective coordination of the CO molecule on the cobalt corrole complex, which does not bind O_2 and N_2.[20] This is also the case for all the organic-inorganic materials incorporating a cobalt(III) corrole complex. As evidenced in Table 2, large specific surface areas and porosities are not the main criteria for large CO volumes adsorbed by the materials described in the present study because even the nonporous **(40Me)M$_1$(Py)$_B$** shows a high affinity for CO with a percentage of active sites similar to the highly porous **(40Me)M$_2$(Py)$_C$** material. Figure 1 gives an example of CO, O_2, and N_2 adsorption isotherms recorded for the **(40T)D$_1$(Py)$_A$** hybrid at 293 K. As previously described for cobalt corrole complexes,[20] the CO adsorption isotherms were analyzed by means of a multiple-site adsorption process involving a double Langmuir plus a single Henry-type adsorption model (Figure 1).[39–41] The first two Langmuir-type isotherms reflect the chemisorption of carbon monoxide, on the one hand, to accessible sites located at the surface of the material with a high energy interaction (V_1 and $(P_{1/2})_1$ in Table 2) and on the other hand, to less energetic binding or less accessible metal sites inside the material (V_2 and $(P_{1/2})_2$ in Table 2). $(P_{1/2})_1$ values are inferior to $(P_{1/2})_2$ ones thus reflecting higher K_1 binding constants than K_2 for all the synthesized hybrids (Table 2). A third Henry-type isotherm was used to describe the physisorption of CO on the material ($K_3 \times 10^3$ in Table 2). Process 1 is predominant in the low-pressure domain (<30 Torr), while processes 2 and 3 mainly occur at higher pressures. As for Co^{III} corrole complexes, the very low $(P_{1/2})_1$ value is in accordance with the very high affinity and selectivity for CO of all the synthesized materials compared to N_2 and O_2. V_{CO}, given in Table 2, corresponds to the experimental volume of CO adsorbed at 760 Torr. Most of the active sites seem to be located at the surface of the materials because the nonporous xerogel, **(40Me)M$_1$(Py)$_B$** (Table 1, entry 3) exhibits a substantial affinity for CO (Table 2, entry 3). Moreover, the use of MTEOS instead of TEOS for **(40Me)M$_1$(Py)$_B$**, **(40Me)M$_2$(Py)$_C$** hybrids does not raise the number of available sites because the percentage of adsorbed CO molecules per cobalt atom ranges from 38 to 41% (Table 2, entries 3–4). Owing to the absence of chemisorption of N_2 and O_2, the

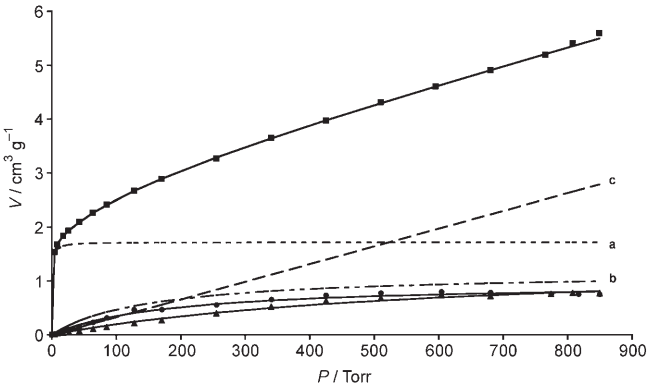

Figure 1. Experimental adsorption isotherms of ■ CO, ▲ N_2 and ● O_2 for **(40T)D$_1$(Py)$_A$** recorded at 293 K; —— calculated isotherms; curves a and b represent the first two components of the calculated isotherm for CO adsorption, and curve c represents Henry-type isotherms for CO adsorption.

Table 2. Experimental and calculated CO adsorption data for the xerogels.

	Material	V_{CO}[a] [cm^3 g^{-1}]	V_1 [cm^3 g^{-1}]	$(P_{1/2})_1$[b] [Torr]	V_2 [cm^3 g^{-1}]	$(P_{1/2})_2$[b] [Torr]	$K_3 \times 10^3$ [Torr^{-1}]	[Co][c] [mmol g^{-1}]	CO[d] [%]
1	**(40T)M$_{1A}$**[e]	5.92	0.54	1.12	0.75	138	6.19	0.186	31
2	**(40T)M$_1$(Py)$_A$**[e]	4.16	1.00	1.22	1.39	141	2.60	0.202	53
3	**(40Me)M$_1$(Py)$_B$**[e]	3.06	1.30	0.40	0.58	73	1.61	0.219	38
4	**(40Me)M$_2$(Py)$_C$**	2.31	0.86	0.76	1	107	0.72	0.201	41
5	**(40T)D$_1$(Py)$_A$**	5.19	1.71	0.68	1.16	147	3.29	0.229	56
6	**(60T)D$_1$(Py)$_A$**	4.57	1.11	1.30	1.28	119	3.04	0.166	64
7	**(80T)D$_1$(Py)$_A$**	3.87	0.88	1.80	5.40	919	–[f]	0.130	30[g]
8	**(100T)D$_1$(Py)$_A$**	3.40	0.73	2.37	9.04	1857	–[f]	0.102	32[g]
9	**(40T)D$_1$(PrN)$_A$**	4.34	2.19	0.30	0.55	76	2.15	0.266	46
10	**(40T)D$_2$(Py)$_B$**	3.69	0.54	0.27	1.32	185	2.75	0.246	33
11	**(40T)D$_2$(PrN)$_A$**	3.48	0.35	0.03	0.46	58	3.47	0.166	22
12	**(40T)D$_3$(Py)$_A$**	3.56	1.07	1.89	1.25	159	2.08	0.283	36
13	**(40T)T$_1$(Py)$_B$**	6.45	1.39	0.12	1.14	65	5.26	0.303	37
14	**(40T)T$_1$(DMeEN)$_B$**	5.13	1.14	0.15	0.98	130	4.12	0.288	33
15	**(40T)T$_2$(Py)$_B$**	4.21	0.85	0.19	1.18	166	3.17	0.290	31

[a] Experimental volume adsorbed at 760 Torr. [b] $(P_{1/2})_i = 1/K_i$. [c] Concentration of cobalt in the materials. [d] Percentage of active sites calculated from $V_1 + V_2$ and [Co]. [e] From ref. [21]. [f] A double Langmuir-type isotherm model was used. [g] Percentage of active sites calculated from V_1 and [Co].

adsorption of these gases is described well by a single Langmuir-type isotherm (Table S1) related to their nonselective physisorption by the silica matrix.

The CO adsorption characteristics of the xerogels prepared from TEOS and difunctionalized complexes are significantly enhanced with respect to those prepared under the same experimental conditions with monofunctionalized derivatives. For example, **(40T)D_1(Py)$_A$**, **(40T)D_1(PrN)$_A$**, and **(40T)M_1(Py)$_A$**, obtained under strictly identical experimental conditions, exhibit similar V_{CO} and % CO data (Table 2, entries 2, 5, 9); however, the V_1/V_2 ratio significantly increases for the difunctionalized corroles which results from a higher accessibility of the Co^{III} sites in these solids and thus reflects a predominance of the higher energy-adsorption contribution.

Furthermore, a partial loss of activity is observed for the most diluted cogels (from 40 to 100 equivalents of TEOS (Table 2, entries 5–8), as far as the percentage of active sites is concerned. However, no important effect is noticed when exchanging Py for PrN as a protecting ligand (Table 2, entries 5 and 9).

Conversely, there are noticeable differences when differently substituted corrole macrocycles are used. It is noteworthy that for the most diluted materials (Table 2, entries 7 and 8), only a double Langmuir-type model was applied, the first one reflecting the chemisorption process of CO and the second one describing the physisorption of CO on the material. This result demonstrates the higher accessibility of the metal sites as the dilution rate increases.

The efficacy of the material (% CO bound by the cobalt corrole) decreases as the Lewis acid character of the central Co^{III} ion increases (Table 2, entries 2, 5, 9–12). For example, **(40T)D_2(PrN)$_A$**, obtained from the cobalt corrole complex **D_2** bearing Cl atoms at the *ortho* positions of 2 *meso*-phenyl groups, exhibits half the efficacy of the material **(40T)D_1(PrN)$_A$**, whose cobalt corrole complex bears methyl groups at the same positions (22 and 46%, respectively). This decrease in efficacy of the hybrid materials results from a greater interaction of the metal sites with silanol or siloxane groups located on the surface of the solid material for the metallocorrole possessing the largest Lewis character. Indeed, the more electron-poor the metal is, the stronger is the interaction with the surface. Moreover, it is noteworthy that, for materials prepared from complexes **D_2** and **D_3**, the V_2 volume is larger than V_1 (Table 2, entries 10–12). This further demonstrates that the enhanced Lewis acid character of complexes **D_2** and **D_3** compared to **D_1** leads to increasing interactions of those complexes with the surface of the materials. Variation of the length of the anchoring arm has almost no influence on the efficacy of the materials.

When trifunctionalized complexes are incorporated into the solid matrix, the efficacy of the resulting materials is slightly below than that observed for the difunctionalized analogues (Table 2, entries 5 and 13, and entries 9 and 14) if one considers the percentage of active sites and the V_1 adsorbed volume, while maintaining a very high selectivity for CO with respect to N_2 and O_2 (Table 2, entries 13–15).

Fifteen organic–inorganic hybrid materials were synthesized by means of the sol–gel process. Many parameters, such as the nature of the cobalt corrole complex, the co-polycondensation agent, the metal-protecting ligand added during the gelation process, and the reaction conditions, were changed for the preparation of the materials. In all cases, very high selectivities were found for CO compared to N_2 and O_2, which makes them of great interest for CO detection. However, the efficacy (% CO in Table 2) could not be raised above 65%, even if the addition of a protecting ligand during the gelation reaction greatly enhanced this factor. The removal of this ligand after the gelation process releases a cavity around the cobalt ion that favors coordination of the carbon monoxide molecule but, nevertheless, does not avoid any further interaction of Co^{III} with the silanol and siloxane functions of the material.

Incorporation of cobalt(III) corroles in a mesoporous silica of the type SBA-15

Preparation of the materials: Six organic-inorganic hybrid materials were obtained by grafting cobalt corrole complexes onto SBA-15 mesoporous silica. The formulation of the materials is given in Scheme 4. This mesostructured

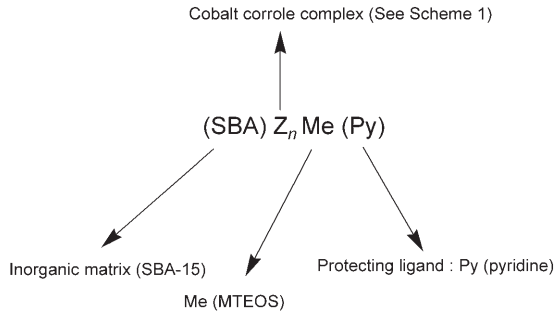

Scheme 4. Formulation used for the SBA-15-based materials incorporating Co^{III} corroles. Example: **(SBA)M_2Me(Py)**: $Z_n = M_2$ (monofunctionalized complex **M_2**).

silica was synthesized as described in the literature[30,31] by hydrolysis and polycondensation of TEOS in an acidic medium in the presence of the Pluronic P123 triblock copolymer surfactant as a structure-directing agent. This silica exhibits a two-dimensional hexagonal structure with a narrow pore size distribution. The cylindrical pores, centered at $D_p \approx 82$ Å, are large enough to incorporate the corrole ring. The materials were aged for three days at 80°C, followed by removal of the surfactant by washing with methanol, and calcination of the silica at 550°C for 6 h to provide a well-condensed solid. A characteristic feature of the SBA-15 silica is the presence of complementary irregular micropores in the wall of the ordered mesostructure.[42–46]

The postsynthetic functionalization[47–50] of the mesoporous silica was carried out by anchoring the monofunctionalized complexes **M_2** and **M_3** in toluene at 80°C for 24 h in the

presence of a large excess of pyridine (Scheme 5). After filtration, the hybrid material was thoroughly washed with methanol and finally dried under vacuum to remove any trace of pyridine (**(SBA)M_2(Py)**, **(SBA)M_3(Py)**). Two other materials with a more hydrophobic surface were prepared from complexes $\mathbf{M_2}$ and $\mathbf{M_3}$ under the same conditions as before by addition of excess MTEOS after the grafting reaction (Scheme 5). **(SBA)M_2Me(Py)**, **(SBA)M_3Me(Py)** hybrids were obtained after the same treatment as for **(SBA)M_2(Py)** and **(SBA)M_3(Py)** materials. The surface of these latter materials is more hydrophobic owing to the presence of methyl groups (See Scheme 5). **(SBA)D_1(Py)** and **(SBA)D_1Me(Py)** hybrids were synthesized using the same procedure as for monofunctionalized complexes without or with the presence of MTEOS, respectively (Scheme 5).

Characterization of the materials: All the data relating to the texture of the hybrid materials are gathered in Table 3 along with those for the starting SBA-15 silica. The hexagonal structure of the SBA-15 silica as well as those of all the synthesized materials were deduced from powder X-ray diffraction measurements. The grafting of the metallocorrole inside the ordered mesoporous channels of the SBA-15 was monitored by N_2 adsorption measurements at 77 K to determine the decreases in surface area and in the pore diameter compared to the pristine silica. One of the main features of mesoporous silicas prepared in micellar media is their regular hexagonal structure along with a narrow pore distribution. Moreover, organic functionalization has almost no effect on the hexagonal long-range mesoscopic order. The narrow pore size distribution of the mesopores centered at different pore diameter values is given in Figure 2 for **SBA-15**, **(SBA)M_2(Py)**, and **(SBA)M_2Me(Py)** (Table 3).

As expected, a significant decrease in the BET surface area and the mesopore volume is observed upon organic functionalization of the mesoporous silica surface (Table 3 and Figure 2). The same observations can be made for all the hybrid materials described here (Table 3). The extent of such a decrease is dependent on the size of bound groups and the rate of anchoring of the metallocorrole (Table 3 and Table 4). The resulting changes in N_2 adsorption at 77 K are particularly striking for the most hydrophobic solid obtained after surface passivation of the residual silanols by MTEOS. The overall shape of the adsorption isotherms remains unchanged, and the pronounced steps of N_2 capillary condensation in primary mesopores are evident, indicating that ordering of the SBA-15 support is not affected by the modification. However, the position of the capillary condensation

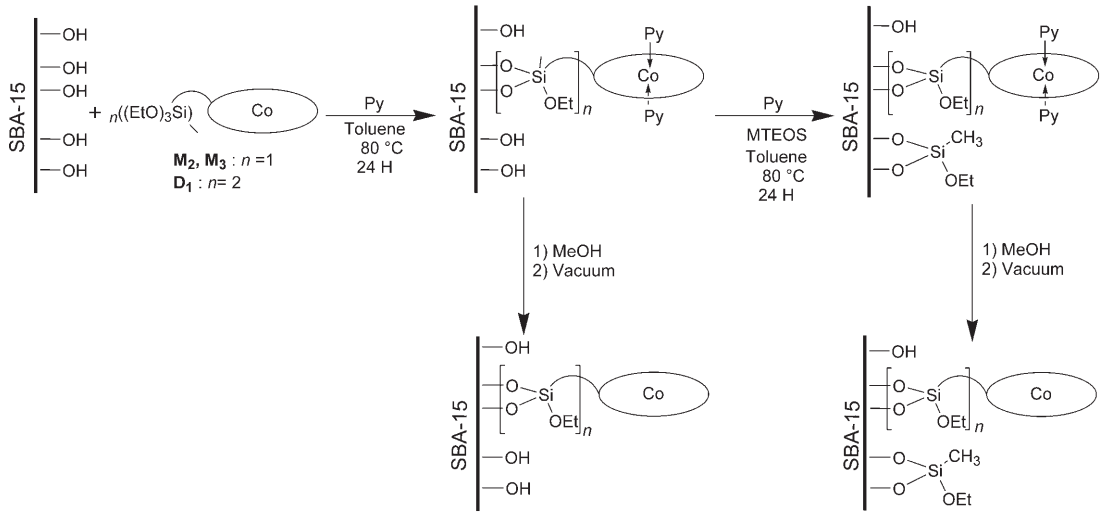

Scheme 5. Reaction scheme to synthesize SBA-15-based materials.

Table 3. Texture characteristics of SBA-15-based materials (a = 112 Å).[a]

	Material	S_{BET}[b] [$m^2 g^{-1}$]	S_m[b] [$m^2 g^{-1}$]	S_p[b] [$m^2 g^{-1}$]	V_t[b] [$cm^3 g^{-1}$]	V_m[b] [$cm^3 g^{-1}$]	V_p[b] [$cm^3 g^{-1}$]	S_m/S_p	D_p[c] [Å]
1	SBA-15	820	303	504	1.02	0.15	0.82	0.60	82
2	**(SBA)M_2(Py)**	451	119	303	0.54	0.05	0.44	0.39	69
3	**(SBA)M_2Me(Py)**	403	47	337	0.46	0.02	0.39	0.14	60
4	**(SBA)M_3(Py)**	473	77	358	0.60	0.04	0.50	0.21	70
5	**(SBA)M_3Me(Py)**	463	95	358	0.60	0.04	0.50	0.26	71
6	**(SBA)D_1(Py)**	587	143	418	0.73	0.08	0.60	0.34	73
7	**(SBA)D_1Me(Py)**	566	122	423	0.71	0.07	0.59	0.29	74

[a] Unit cell parameter determined by XRD measurements. [b] S_{BET}: Total specific surface area; S_m: Specific surface area of the complementary micropores in the silica wall; S_p: specific area of the primary mesopores; V_t: total pore volume; V_m: micropore volume; V_p: mesopore volume. [c] Mesopore diameter determined with the BJH model.

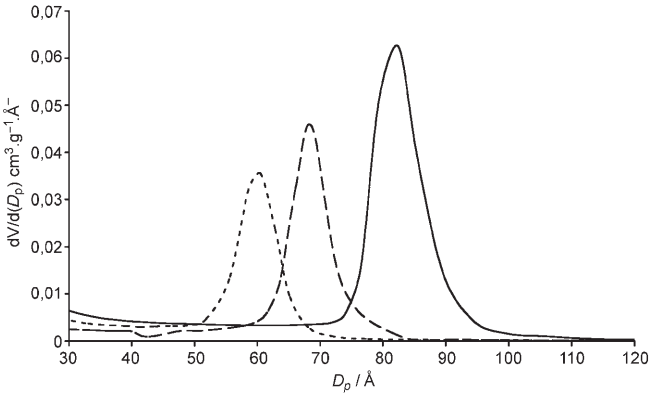

Figure 2. Pore size distribution for the starting **SBA-15** (——), the **(SBA)M$_2$(Py)** (-----), and **(SBA)M$_2$Me(Py)** (•••••) functionalized materials.

steps gradually shifts to lower pressures in accordance with the decrease in the mesopore size.[47,51,52] It was also shown in the literature that the introduction of organosilyl ligands on the silica surface changes the surface properties of the adsorbent with respect to nitrogen molecules, the effect being more pronounced in the case of long-chain or bulky organosilyl groups.[42,53] The primary mesopore and complementary micropore volumes and surfaces as well as the external surface area were thus calculated with the alpha plot method (Table 3).[43,54]

The high specific surface area is not only ascribed to the lowering of the contribution from the large mesopores to the total surface area (BET surface), but also to the contribution of smaller pores located in the walls of the SBA-15. This is evidenced by a large decrease of both micropore and mesopore surfaces and volumes after metallocorrole anchoring (Table 3). However, there is no evidence of pore-blocking effects, as inferred from the resulting microporous and mesoporous surface area and volume, as well as the reversibility of the nitrogen adsorption–desorption isotherms, which indicates that the pore geometry does not deviate from its initial cylindrical shape for SBA-15 materials. Moreover, even if the complementary micropores/mesopores ratio (S_m/S_p) is lowered after functionalization of SBA-15, the complementary micropores are only partially blocked by the metallocorrole. In other words, the large organosilyl moieties do not fill up or block both micropores and mesopores, which ensures a high accessibility of the metal complexes towards CO binding.

The ^{29}Si CP-MAS NMR experiment, performed on the **(SBA)M$_2$Me(Py)** material, clearly indicates the high level of condensation of the inorganic matrix by the presence of Q^3 and Q^4 units at $\delta = -101$ and -110 ppm. The organic part of the material is evidenced by a set of resonances lying at $\delta = -50$, -57, and -65 ppm, which are assigned to T^1, T^2, and T^3 substructures. For all the materials, the removal of the pyridine molecules, used as a protecting ligand for Co^{III} ions during anchoring on the silica surface, is clearly shown by UV/Vis spectroscopy with the absence of the band at about 600 nm related to the hexacoordinate bis(py)cobalt(III) corrole species (see the Experimental Section).[35]

Gas adsorption measurements: Adsorption isotherms for N_2, O_2 and CO were measured for all the SBA-15-based materials. CO adsorption data are summarized in Table 4 and data relative to O_2 and N_2 adsorption are given in Table S2. An example of N_2, O_2, and CO adsorption isotherms is given in Figure 3 for the **(SBA)M$_2$(Py)** material. As for the hybrid xerogels, the process involved in O_2 and N_2 adsorption is physisorption.

The reactivity and selectivity of the SBA-15-based materials with respect to carbon monoxide are similar to those of the hybrid xerogel materials. Indeed, a double Langmuir-type adsorption model to which a Henry isotherm was added to take into account the nonselective adsorption phenomena on the silica surface[20,39–41] gave a perfect fit of the

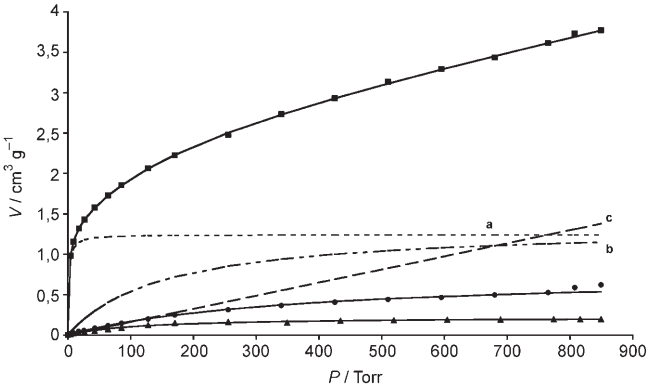

Figure 3. Experimental adsorption isotherms of ■ CO, ▲ N_2 and ● O_2 for (SBA)M$_2$(Py) recorded at 293 K; —— calculated isotherms; curves a and b represent the first two components of the calculated isotherm for CO adsorption, and curve c represents the Henry-type isotherms for CO adsorption.

Table 4. Experimental and calculated CO adsorption data for SBA-15-based materials recorded at 293 K.

	Material	V_{CO}[a] [cm^{3}g]	V_1[b] [cm^{3}g^{-1}]	$(P_{1/2})_1$[c] [Torr]	V_2 [cm^{3}g]	$(P_{1/2})_2$[c] [Torr]	[Co][d] [mmol g^{-1}]	CO[e] [%]
1	**(SBA)M$_2$(Py)**	3.61	1.28	1.76	1.37	169	0.254	46
2	**(SBA)M$_2$Me(Py)**	3.60	1.54	0.91	1.06	64	0.244	48
3	**(SBA)M$_3$(Py)**	4.77	2.70	0.22	1.45	156	0.266	69, 45[f]
4	**(SBA)M$_3$Me(Py)**	4.87	2.33	0.48	2.19	350	0.268	75, 39[f]
5	**(SBA)D$_1$(Py)**	2.68	0.75	0.81	0.94	204	0.132	57
6	**(SBA)D$_1$Me(Py)**	1.75	0.35	0.80	0.38	100	0.078	41

[a] Experimental volume adsorbed at 760 Torr. [b] Calculated volume for the i^{th} contribution. [c] $(P_{1/2})_i = 1/K_i$. [d] Concentration of cobalt in the materials. [e] Percentage of active sites calculated from $V_1 + V_2$ and [Co]. [f] Percentage of active sites calculated from V_1 and [Co].

CO adsorption isotherm (Figure 3). The first two Langmuir-type isotherms represent the chemisorption of carbon monoxide. As a whole, the hybrids are highly selective for CO compared to O_2 and N_2, especially in the low-pressure domain, the percentage of active cobalt sites ranges between 40 and 60% (Table 4). Although the metallocorroles are included in the mesopores of an open framework, the reactivity is quite similar to that observed for the xerogel materials (See Table 2). Treatment of the silica surface with MTEOS after grafting of the cobalt corrole complex does not significantly improve the performance of the materials towards CO if one considers both the adsorption capacity (V_1) and the percentage of active sites. Data reported in Table 4 are close to those gathered in Table 2 for the xerogel materials and this therefore demonstrates that all the reported materials exhibit very high efficacies and almost infinite selectivities for CO towards O_2 and N_2. However, there is no direct correlation between the affinity and capacity of the materials for CO binding and their porosity.

Conclusion

Twenty-one hybrid materials incorporating cobalt(III) corrole complexes were synthesized by either a sol–gel process or by grafting onto mesostructured silica of the SBA-15 type. All the materials exhibited an almost infinite selectivity for CO with respect to N_2 and O_2 in the low-pressure domain where the chemisorption phenomenon is predominant. This selectivity slightly decreases at high pressures where nonselective physisorption phenomena mainly occur. Moreover, it has to be noted that dihydrogen adsorption experiments carried out on all the materials demonstrated that neither type of material adsorbed H_2 nor was structurally affected by this gas.[55] Furthermore, CO adsorption reversibility experiments, carried out on 10 cycles for each material, clearly indicated a good reproducibility of the gas adsorption during the cycles, which resulted in the high reversibility of the solid–gas adsorption reaction.

The percentage of active sites in the CO chemisorption process ranges from 22 to 64% and cannot exceed this latter value. This may be a consequence of interactions between the cobalt(III) corroles with silanol or siloxane groups remaining at the surface of the materials thus preventing further coordination of the CO molecule. Notably, the most efficient materials were those prepared in the presence of a protecting ligand during the gelation or the grafting process. The stability of the SBA-15 hybrid was explored over a period of several months, and it was shown that the CO adsorption properties were not affected. Conversely, the xerogel material capacities slowly decreased owing to evolution of the material structure.

Future developments under consideration include direct incorporation of the corrole complex inside the walls of mesoporous silica from a direct synthesis in micellar medium. Such materials would exhibit structural and textural stabilities allowing long-term use of the material. Finally, other solid supports will be used, such as organic polymers, that should prevent interactions between the cobalt corrole complexes and the silica surface of the material thus inducing a decrease in the chemisorption of CO.

Experimental Section

General: The characterization of the cobalt(III) corrole complexes was performed by UV/Vis spectroscopy with a Varian Cary 50 spectrophotometer and by mass spectrometry either on a KRATOS Concept 32S at 70 eV (EI) and or on a BRUKER ProFLEX III spectrometer (MALDI/TOF) using dithranol as the matrix. The hybrid materials were characterized by means of the following techniques: ^{29}Si CP MAS NMR spectra were recorded on a BRUKER FTAM 300 at the University of Montpellier II. Chemical shifts are given in ppm and are expressed relative to tetramethylsilane (TMS). The ^{29}Si CP MAS frequency was 56.62 MHz, repetition time 10 s, contact time 2 ms, and rotation rate 5 kHz. Solid-state UV/Vis spectra were recorded in the diffuse reflectance mode on a VARIAN Cary 500 equipped with a Spectralon® integration sphere DRA-CA-50 (LABSPHERE). Powder samples (5–10 mg) were ground and dispersed in a silica gel matrix (300 mg, Kieselgel MERCK 10184). IR spectra measurements were performed on a BRUKER FT-IR IFS 66v, equipped with a P/N 19900 (GRASEBY SPECAC) accessory, in the diffuse reflectance mode. Solid samples were dispersed in silica gel (Kieselgel MERCK 10184). The baseline spectrum was obtained from pure silica gel. C, H, N, and S microanalyses were performed on a FISONS EA 1108 CHNS instrument while Co and Si microanalyses were obtained from the "Service Central d'Analyses du CNRS, Lyon". Powder X-ray diffraction experiments were carried out on a BRUKER D 5000 diffractometer at the University of Montpellier II. The diffractometer was equipped with a rotating anode and used $Cu_{K\alpha}$ radiation. Textural data were obtained from N_2 adsorption measurements performed at 77 K with adsorption/desorption cycles between 0.01 and 760 Torr, each sample being previously degassed by heating under vacuum (10^{-3} Torr) at 100 °C. Specific surface areas were measured by the Brunauer–Emmet–Teller method (BET)[37] on a MICROMERITICS ASAP 2010 analyzer in the relative P/P_0 pressure range from 0.05 to 0.25. The cross-sectional area of the nitrogen molecule was assumed to be equal to 0.162 nm^2. The total pore volume, V_t, was evaluated on the basis of the amount adsorbed at the relative pressure of about 0.99. The primary mesopore volume, V_p, the complementary micropore volume, V_m, and their respective surface areas were evaluated by means of the α plot method[54] using a macroporous silica as a reference adsorbent. Average pore diameters were calculated by the Barrett–Joyner–Halenda method (BJH)[38] with an uncorrected form of the Kelvin equation, that is, using a standard statistical film thickness curve. N_2, O_2, and CO adsorption experiments performed at 293 K were run with the same instrument with a 60 s equilibration delay. The equilibrium constants for the gas-binding affinity, K_i, and the adsorption capacity, V_i, were calculated by considering two different adsorption processes: a selective chemisorption on the Co^{III} ion and a nonselective physisorption resulting from dissolution and diffusion of the gas into the solid material.[20] The experimental isotherms corresponding to CO adsorption were thus analyzed by means of a model based on two Langmuir-type isotherms [Eq. (1)] to which is added a Henry-type isotherm, and the N_2 and O_2 isotherms are fitted with a single Langmuir-type isotherm model [Eq. (2)].

$$V_{CO} = \frac{V_1 K_1 P}{1 + K_1 P} + \frac{V_2 K_2 P}{1 + K_2 P} + K_3 P \quad (1)$$

$$V_{N_2} \text{ or } V_{O_2} = \frac{V_1 K_1 P}{1 + K_1 P} \quad (2)$$

where $K_i = 1/(P_{1/2})$

The thermogravimetric analyses (TGA/MS) were carried out on a NETZSCH STA 409 PC thermobalance coupled with a mass detector FISONS GAS LAB 300. A 20 to 50 mg sample of the material was intro-

duced in an alumina crucible and then heated from 25 to 1200 °C (10 K min^{-1}) under a stream of Ar (30 mL min^{-1}) and O_2 (10 mL min^{-1}).

All reagents of analytical grade were obtained from commercial suppliers (Acros or Aldrich) and used without further purification. Solvents were thoroughly distilled before use: dichloromethane over CaH_2, ethanol over Mg turnings, and pyridine over KOH, THF and toluene over benzophenone/sodium complex.

General synthesis of cobalt(III) corroles

The free corrole base[29] (0.2 mmol) and cobalt(II) acetylacetonate (0.25 mmol, 1.25 equiv) were dissolved in dry dichloromethane (21 mL) and dry ethanol (9 mL) under argon. The mixture was stirred and refluxed for 24 h. The reaction was monitored by UV/Vis spectroscopy and mass spectrometry. After evaporation, the complex was recrystallized from a mixture of dichloromethane, ethanol, and heptane, which was then filtered, washed with pentane, and dried under vacuum.

[5,15-Dimesityl-10-{4-[3-(3-triethoxysilylpropyl)ureidomethyl]-phenyl}corrolato]cobalt(III) (M_2): Yield: 97%; UV/Vis (CH_2Cl_2): λ_{max} (ε) = 389 nm (41700 mol^{-1} dm^3 cm^{-1}); UV/Vis (pyridine): λ_{max} (ε) = 438 (44600), 456 (40700), 585 (14900), 624 nm (18800 mol^{-1} dm^3 cm^{-1}); MS (MALDI/TOF): *m/z* (%): 943.06 (100) $[M+H]^+$; elemental analysis calcd (%) for $C_{54}H_{59}CoN_6O_4Si\cdot CH_2Cl_2$: C 64.26, H 5.98, N 8.17; found: C 64.64, H 5.79, N 8.29.

[5,15-Bis(2,6-dichlorophenyl)-10-{4-[3-(3-triethoxysilylpropyl)ureidomethyl]phenyl}corrolato]cobalt(III) (M_3): Yield: 98%; UV/Vis (CH_2Cl_2): λ_{max} (ε) = 391 nm (42400 mol^{-1} dm^3 cm^{-1}); MS (MALDI/TOF): *m/z* (%): 997.68 (100) $[M+H]^+$; elemental analysis calcd (%) for $C_{48}H_{43}Cl_4CoN_6O_4Si\cdot CH_2Cl_2$: C 54.41, H 4.19, N 7.77; found: C 54.81, H 4.36, N 8.25.

[5,15-Bis{2,6-dimethyl-4-[(3-triethoxysilylpropyl)aminocarbonyloxy]phenyl}-10-(4-cyanophenyl)corrolato]cobalt(III) (D_1): Yield: 93%; UV/Vis (CH_2Cl_2): λ_{max} (ε) = 387 nm (47900 mol^{-1} dm^3 cm^{-1}); MS (MALDI/TOF): *m/z* (%): 1189.21 (100) $[M]^{+\cdot}$; elemental analysis calcd (%) for $C_{62}H_{72}CoN_7O_{10}Si_2\cdot CH_2Cl_2$: C 59.33, H 5.85, N 7.69; found: C 59.01, H 6.06, N 7.56.

[5,15-Bis{2,6-dichloro-4-[(3-triethoxysilylpropyl)aminocarbonyloxy]phenyl}-10-(4-cyanophenyl)corrolato]cobalt(III) (D_2): Yield: 95%; UV/Vis (CH_2Cl_2): λ_{max} (ε) = 394 nm (51100 mol^{-1} dm^3 cm^{-1}); UV/Vis (CH_2Cl_2/pyridine, 99:1): λ_{max} (ε) = 444 (46800), 455 (46800), 540 (8400), 587 (9700), 617 (19000), 726 nm (7100 mol^{-1} dm^3 cm^{-1}); UV/Vis (CH_2Cl_2/propylamine, 99:1): λ_{max} (ε) = 443 (51200), 460 (47500), 543 (8700), 588 (10700), 619 (20700), 726 nm (8300 mol^{-1} dm^3 cm^{-1}); MS (MALDI/TOF): *m/z* (%): 1269.41 (100) $[M]^{+\cdot}$; elemental analysis calcd (%) for $C_{58}H_{60}Cl_4CoN_7O_{10}Si_2\cdot 1.5\,CH_2Cl_2$: C 51.07, H 4.54, N 7.01; found: C 51.04, H 4.71, N 7.57.

[5,15-Bis{2,6-dichloro-4-[2-(3-triethoxysilylpropylureido)ethoxy]phenyl}-10-(4-fluorophenyl)corrolato]cobalt(III) (D_3): Yield: 91%; UV/Vis (CH_2Cl_2): λ_{max} (ε) = 405 nm (22500 mol^{-1} dm^3 cm^{-1}); MS (MALDI/TOF): *m/z* (%): 1348.40 (100) $[M]^{+\cdot}$; elemental analysis calcd (%) for $C_{61}H_{70}Cl_4CoFN_8O_{10}Si_2\cdot CH_2Cl_2$: C 51.85, H 5.05, N 7.80; found: C 51.84, H 5.37, N 7.69.

[5,15-Bis{2,6-dimethyl-4-[(3-triethoxysilylpropyl)aminocarbonyloxy]phenyl}-10-{4-[(3-triethoxysilylpropyl)aminocarbonyloxy]phenyl}corrolato]-cobalt(III) (T_1): Yield: 91%; UV/Vis (CH_2Cl_2): λ_{max} (ε) = 404 nm (53500 mole^{-1} dm^3 cm^{-1}); UV/Vis (CH_2Cl_2/pyridine, 99:1): λ_{max} (ε) = 429 (56400), 452 (33000), 538 (7400), 583 (7600), 620 nm (21000 mol^{-1} dm^3 cm^{-1}); UV/Vis (CH_2Cl_2/propylamine, 99:1): λ_{max} (ε) = 424 (64400), 455 (45300), 538 (7600), 585 (9800), 622 nm (22400 mol^{-1} dm^3 cm^{-1}); MS (MALDI/TOF): *m/z* (%): 1427.93 (1OO) $[M]^{+\cdot}$; elemental analysis calcd (%) for $C_{71}H_{94}CoN_7O_{15}Si_3\cdot 1.5\,CH_2Cl_2$: C 55.96, H 6.28, N 6.30; found: C 55.87, H 6.19, N 6.95.

[5,15-Bis{2,6-dichloro-4-[(3-triethoxysilylpropyl)aminocarbonyloxy]phenyl}-10-{4-[(3-triethoxysilylpropyl)aminocarbonyloxy]phenyl}corrolato]-cobalt(III) (T_2): Yield: 91%; UV/Vis (CH_2Cl_2): λ_{max} (ε) = 392 nm (29700 mol^{-1} dm^3 cm^{-1}); UV/Vis (CH_2Cl_2/pyridine, 99:1): λ_{max} (ε) = 440 (41000), 454 (37300), 589 (11500), 621 nm (17100 mol^{-1} dm^3 cm^{-1}); UV/Vis (CH_2Cl_2/propylamine, 99:1): λ_{max} (ε) = 439 (48100), 456 (41000), 591 (14500), 623 nm (20600 mol^{-1} dm^3 cm^{-1}); MS (MALDI/TOF): *m/z* (%): 1509.39 (100) $[M]^{+\cdot}$; elemental analysis calcd (%) for $C_{67}H_{82}Cl_4CoN_7O_{15}Si_3\cdot 2\,CH_2Cl_2$: C 49.38, H 5.04, N 5.84; found: C 49.41, H 5.51, N 6.53.

Preparation of xerogels

(40T)M_{1A}, **(40T)M_1(Py)$_A$** and **(40Me)M_1(Py)$_B$** were obtained according to the previously reported procedure.[21]

(40Me)M_2(Py)$_C$: Cobalt(III) corrole $\mathbf{M_2}$ (170 mg, 0.18 mmol) and methyltriethoxysilane (1.285 g, 7.21 mmol, 40 equiv) were dissolved in dry pyridine (11 mL). The mixture was stirred at room temperature for 5 min and then heated to 110 °C before distilled water (199 μL, 11.05 mmol, 61.5 equiv) and a 1 M solution of TBAF (369 μL, 0.369 mmol, 5%/Si) were added simultaneously. The solution was stirred for 5 min at 110 °C until a dark green gel had formed. The gel was allowed to age at 110 °C for three days before it was filtered, powdered, and washed thoroughly with methanol, dichloromethane, heptane, and pentane. The brown solid was then dried under vacuum to yield 501 mg (90%) of **(40Me)M_2(Py)$_C$**. S_{BET} = 523 ± 9 m^2 g^{-1}; ^{29}Si NMR CP/MAS (60 MHz, 25 °C, TMS) : δ = −68.0 ppm(T^3); IR (KBr): $\tilde{\nu}$ = 3480 (νH-bonded O-H), 2978 (νC_{sp^3}-H), 1634 (δO-H (H_2O)), 1544 (δN-H), 1273 (νSi-CH_3), 1200–1050 (νSi-O-Si), 782 cm^{-1} (δSi-OH); UV/Vis (diffuse reflectance): λ_{max} = 391 nm; elemental analysis calcd (%) for $C_{88}H_{164}CoN_6O_{62.5}Si_{41}$ with $n(H_2O)$ = 10.76: C 28.48, H 5.04, N 2.26, Si 31.03, Co 1.59; found: C 28.44, H 4.88, N 2.19, Si 33.59, Co 1.19.

(40T)D_1(Py)$_A$: Cobalt(III) corrole $\mathbf{D_1}$ (200 mg, 0.17 mmol), tetraethoxysilane (1.400 g, 6.72 mmol, 40 equiv), and dry pyridine (0.5 mL, 6.13 mmol, 36 equiv) were dissolved in dry tetrahydrofuran (8 mL). The dark green mixture was stirred at room temperature for 5 min before distilled water (251 μL, 13.95 mmol, 83 equiv) and a 1 M solution of TBAF (70.6 μL, 0.07 mmol, 1%/Si) were added simultaneously. The solution was stirred for 5 min at room temperature until a dark green gel had formed. The gel was allowed to age at 25 °C for seven days before it was filtered, powdered, and washed thoroughly with methanol, dichloromethane, heptane, and pentane. The brown solid was then dried under vacuum to yield 602 mg (100%) of **(40T)D_1(Py)$_A$**. S_{BET} = 513 ± 10 m^2 g^{-1}; IR (KBr): $\tilde{\nu}$ = 3435 (νH-bonded O-H), 2979, 2931, 2868 (νC_{sp^3}-H), 2232 (νC≡N), 1720 (νC=O), 1632 (δO-H (H_2O)), 1532 (δN-H), 1200–1050 (νSi-O-Si), 958 (νSi-OH), 798 (δSi-OH), 452 cm^{-1} (δSi-O-Si); UV/Vis (diffuse reflectance): λ_{max} = 395 nm; anal. found (%) for $C_{50}H_{42}CoN_7O_{87}Si_{42}$: C 16.93, H 2.29, N 2.64, Si 32.83, Co 1.35; calcd with $n(H_2O)$ = 12.60: C 16.69, H 1.88, N 2.72, Si 32.78, Co 1.64.

(60T)D_1(Py)$_A$: This xerogel was prepared as described for **(40T)D_1(Py)$_A$** from cobalt(III) corrole $\mathbf{D_1}$ (134 mg, 0.11 mmol), tetraethoxysilane (1.400 g, 6.72 mmol, 60 equiv), dry pyridine (0.5 mL, 6.13 mmol, 55 equiv), dry tetrahydrofuran (8 mL), distilled water (249 μL, 13.84 mmol, 123 equiv), and a 1 M solution of TBAF (69.8 μL, 0.07 mmol, 1%/Si) to yield 562 mg (100%) of **(60T)D_1(Py)$_A$** as a dark brown solid. S_{BET} = 563 ± 16 m^2 g^{-1}; IR (KBr): $\tilde{\nu}$ = 3417 (νH-bonded O-H), 2236 (νC≡N), 1711 (νC=O), 1631 (δO-H (H_2O)), 1539 (δN-H), 1200–1050 (νSi-O-Si), 957 (νSi-OH), 798 (δSi-OH), 465 cm^{-1} (δSi-O-Si); UV/Vis (diffuse reflectance): λ_{max} = 399 nm; elemental analysis calcd for $C_{50}H_{42}CoN_7O_{127}Si_{62}$ with $n(H_2O)$ = 14.72: C 12.41, H 1.49, N 2.03, Si 35.99, Co 1.22; found: C 12.99, H 2.22, N 1.99, Si 33.41, Co 0.98.

(80T)D_1(Py)$_A$: This xerogel was prepared as described for **(40T)D_1(Py)$_A$** from cobalt(III) corrole $\mathbf{D_1}$ (100 mg, 0.084 mmol), tetraethoxysilane (1.400 g, 6.72 mmol, 80 equiv), dry pyridine (0.5 mL, 6.13 mmol, 73 equiv), dry tetrahydrofuran (8 mL), distilled water (247 μL, 13.69 mmol, 163 equiv) and a 1 M solution of TBAF (68.9 μL, 0.07 mmol, 1%/Si) to yield 510 mg (100%) of **(80T)D_1(Py)$_A$** as a dark brown solid. S_{BET} = 509 ± 15 m^2 g^{-1}; IR (KBr): $\tilde{\nu}$ = 3429 (νH-bonded O-H), 2237 (νC≡N), 1705 (νC=O), 1635 (δO-H (H_2O)), 1541 (δN-H), 1200–1050 (νSi-O-Si), 960 (νSi-OH), 797 (δSi-OH), 459 cm^{-1} (δSi-O-Si); UV/Vis (diffuse reflectance): λ_{max} = 407 nm; elemental analysis calcd for $C_{50}H_{42}CoN_7O_{167}Si_{82}$ with $n(H_2O)$ = 18.47: C 9.83, H 1.30, N 1.61, Si 37.71, Co 0.96; found: C 10.71, H 2.15, N 1.45, Si 34.72, Co 0.77.

(100T)D_1(Py)$_A$: This xerogel was prepared as described for **(40T)D_1(Py)$_A$** from cobalt(III) corrole $\mathbf{D_1}$ (80 mg, 0.067 mmol), tetraethoxysilane (1.400 g, 6.72 mmol, 100 equiv), dry pyridine (0.5 mL, 6.13 mmol, 91 equiv), dry tetrahydrofuran (8 mL), distilled water

(246 μL, 13.64 mmol, 203 equiv) and a 1 M solution of TBAF (68.6 μL, 0.07 mmol, 1 %/Si) to yield 470 mg (100 %) of **(100 T)D$_1$(Py)$_A$** as a dark brown solid. $S_{BET}=556\pm18\ m^2g^{-1}$; IR (KBr): $\tilde{\nu}=3423$ (νH-bonded O-H), 2237 (νC≡N), 1703 (νC=O), 1633 (δO-H (H_2O)), 1532 (δN-H), 1200–1050 (νSi-O-Si), 959 (νSi-OH), 797 (δSi-OH), 465 cm^{-1} (δSi-O-Si); UV/Vis (diffuse reflectance): $\lambda_{max}=405$ nm; elemental analysis calcd (%) for $C_{50}H_{42}CoN_7O_{207}Si_{102}$ with $n(H_2O)=45.70$: C 7.70, H 1.72, N 1.26, Si 36.73, Co 0.76; found: C 8.09, H 2.03, N 1.17, Si 35.16, Co 0.60.

(40T)D$_1$(PrN)$_A$: This xerogel was prepared as described for **(40T)D$_1$(Py)$_A$** from cobalt(III) corrole **D$_1$** (200 mg, 0.17 mmol), tetraethoxysilane (1.400 g, 6.72 mmol, 40 equiv), propylamine (0.5 mL, 6.0 mmol, 35 equiv), dry tetrahydrofuran (8 mL), distilled water (251 μL, 13.84 mmol, 83 equiv) and a 1 M solution of TBAF (70.6 μL, 0.07 mmol, 1 %/Si) to yield 635 mg (100 %) of **(40T)D$_1$(PrN)$_A$** as a dark brown solid. $S_{BET}=310\pm6\ m^2g^{-1}$; IR (KBr): $\tilde{\nu}=3402$ (νH-bonded O-H), 2979 (νC_{sp^3}-H), 2234 (νC≡N), 1729 (νC=O), 1632 (δO-H (H_2O)), 1200–1050 (νSi-O-Si), 797 (δSi-OH), 458 cm^{-1} (δSi-O-Si); UV/Vis (diffuse reflectance): $\lambda_{max}=412$ nm; elemental analysis calcd (%) for $C_{50}H_{42}CoN_7O_{87}Si_{42}$ with n-(H_2O)=12.38: C 16.71, H 1.87, N 2.73, Si 32.82, Co 1.64; found: C 17.05, H 2.44, N 2.57, Si 32.31, Co 1.57.

(40T)D$_2$(Py)$_B$: This xerogel was prepared as described for **(40T)D$_1$(Py)$_A$** from cobalt(III) corrole **D$_2$** (160 mg, 0.13 mmol), tetraethoxysilane (1.05 g, 5.04 mmol, 40 equiv), dry pyridine (0.5 mL, 6.13 mmol, 49 equiv), dry tetrahydrofuran (8 mL), distilled water (188 μL, 10.44 mmol, 83 equiv) and a 1 M solution of TBAF (264.6 μL, 0.26 mmol, 5 %/Si) to yield 550 mg (93 %) of **(40T)D$_2$(Py)$_B$** as a dark brown solid. $S_{BET}=363\pm9\ m^2g^{-1}$; IR (KBr): $\tilde{\nu}=3410$ (νH-bonded O-H), 2236 (νC≡N), 1629 (δO-H (H_2O)), 1570 (δN-H), 1200–1050 (νSi-O-Si), 955 (νSi-OH), 802 (δSi-OH), 453 cm^{-1} (δSi-O-Si); UV/Vis (diffuse reflectance): $\lambda_{max}=416$ nm; elemental analysis calcd (%) for $C_{46}H_{30}CoCl_4N_7O_{87}Si_{42}$: C 16.00, H 0.88, N 2.84, Si 34.16, Co 1.71; found: C 10.76, H 1.99, N 1.86, Si 38.36, Co 1.45.

(40T)D$_2$(PrN)$_A$: This xerogel was prepared as described for **(40T)D$_1$(Py)$_A$** from cobalt(III) corrole **D$_2$** (213 mg, 0.17 mmol), tetraethoxysilane (1.400 g, 6.72 mmol, 40 equiv), propylamine (0.5 mL, 6.0 mmol, 35 equiv), dry tetrahydrofuran (8 mL), distilled water (251 μL, 13.84 mmol, 83 equiv) and a 1 M solution of TBAF (70.6 μL, 0.07 mmol, 1 %/Si) to yield 550 mg (95 %) of **(40T)D$_2$(PrN)$_A$** as a dark brown solid. $S_{BET}=355\pm12\ m^2g^{-1}$; IR (KBr): $\tilde{\nu}=3417$ (νH-bonded O-H), 2236 (νC≡N), 1631 (δO-H (H_2O)), 1200–1050 (νSi-O-Si), 953 (νSi-OH), 800 (δSi-OH), 462 cm^{-1} (δSi-O-Si); UV/Vis (diffuse reflectance): $\lambda_{max}=428$ nm; elemental analysis calcd (%) for $C_{46}H_{30}CoCl_4N_7O_{87}Si_{42}$: C 16.00, H 0.88, N 2.84, Si 34.16, Co 1.71; found: C 6.82, H 1.86, N 1.42, Si 37.59, Co 0.98.

(40T)D$_3$(Py)$_A$: This xerogel was prepared as described for **(40T)D$_1$(Py)$_A$** from cobalt(III) corrole **D$_3$** (154 mg, 0.11 mmol), tetraethoxysilane (0.950 g, 4.56 mmol, 40 equiv), dry pyridine (0.5 mL, 6.13 mmol, 54 equiv), dry tetrahydrofuran (8 mL), distilled water (170.3 μL, 9.46 mmol, 83 equiv) and a 1 M solution of TBAF (47.9 μL, 0.05 mmol, 1 %/Si) to yield 408 mg (100 %) of **(40T)D$_3$(Py)$_A$** as a dark brown solid. $S_{BET}=419\pm10\ m^2g^{-1}$; IR (KBr): $\tilde{\nu}=3435$ (νH-bonded O-H), 2976, 2927, 2849 (νC_{sp^3}-H), 1635 (δO-H (H_2O)), 1551 (δN-H), 1200–1050 (νSi-O-Si), 956 (νSi-OH), 801 (δSi-OH), 454 cm^{-1} (δSi-O-Si); UV/Vis (diffuse reflectance): $\lambda_{max}=405$ nm; elemental analysis calcd (%) for $C_{49}H_{40}Cl_4CoFN_8O_{87}Si_{42}$ with $n(H_2O)=3.27$: C 16.39, H 1.31, N 3.12, Si 32.85, Co 1.64; found: C 16.93, H 2.15, N 2.95, Si 31.52, Co 1.41.

(40T)T$_1$(Py)$_B$: This xerogel was prepared as described for **(40T)D$_1$(Py)$_A$** from cobalt(III) corrole **T$_1$** (180 mg, 0.13 mmol), tetraethoxysilane (1.050 g, 5.04 mmol, 40 equiv), dry pyridine (0.5 mL, 6.13 mmol, 49 equiv), dry tetrahydrofuran (8 mL), distilled water (192 μL, 10.67 mmol, 84.5 equiv) and a 1 M solution of TBAF (271 μL, 0.27 mmol, 5 %/Si) to yield 498 mg (100 %) of **(40T)T$_1$(Py)$_B$** as a dark brown solid. $S_{BET}=474\pm9\ m^2g^{-1}$; IR (KBr): $\tilde{\nu}=3418$ (νH-bonded O-H), 1720 (νC=O), 1630 (δO-H (H_2O)), 1532 (δN-H), 1200–1050 (νSi-O-Si), 957 (νSi-OH), 798 (δSi-OH), 461 cm^{-1} (δSi-O-Si); UV/Vis (diffuse reflectance): $\lambda_{max}=426$ nm; elemental analysis calcd (%) for $C_{53}H_{49}CoN_7O_{90.5}Si_{43}$: C 18.20, H 1.41, N 2.80, Si 34.52, Co 1.68; found: C 17.00, H 2.56, N 2.47, Si 33.85, Co 1.79;

(40T)T$_1$(DMeEN)$_B$: This xerogel was prepared as described for **(40T)D$_1$(Py)$_A$** from cobalt(III) corrole **T$_1$** (180 mg, 0.13 mmol), tetraethoxysilane (1.050 g, 5.04 mmol, 40 equiv), dimethylethylamine (0.5 mL, 4.58 mmol, 37 equiv), dry tetrahydrofuran (8 mL), distilled water (192 μL, 10.67 mmol, 84.5 equiv) and a 1 M solution of TBAF (271 μL, 0.27 mmol, 5 %/Si) to yield 487 mg (100 %) of **(40T)T$_1$(DMeEN)$_B$** as a dark brown solid. $S_{BET}=431\pm7\ m^2g^{-1}$; IR (KBr): $\tilde{\nu}=3414$ (νH-bonded O-H), 2980 (νC_{sp^3}-H), 1630 (δO-H (H_2O)), 1200–1050 (νSi-O-Si), 961 (νSi-OH), 795 (δSi-OH), 452 cm^{-1} (δSi-O-Si). UV/Vis (diffuse reflectance): $\lambda_{max}=426$ nm; elemental analysis calcd (%) for $C_{53}H_{49}CoN_7O_{90.5}Si_{43}$ with $n(H_2O)=4$: C 17.83, H 1.61, N 2.75, Si 33.82, Co 1.65; found: C 15.64, H 2.38, N 2.36, Si 35.21, Co 1.70.

(40T)T$_2$(Py)$_B$: This xerogel was prepared as described for **(40T)D$_1$(Py)$_A$** from cobalt(III) corrole **T$_2$** (190 mg, 0.13 mmol), tetraethoxysilane (1.050 g, 5.04 mmol, 40 equiv), dry pyridine (0.5 mL, 6.13 mmol, 49 equiv), dry tetrahydrofuran (8 mL), distilled water (192 μL, 10.67 mmol, 84.5 equiv) and a 1 M solution of TBAF (271 μL, 0.27 mmol, 5 %/Si) to yield 498 mg (100 %) of **(40T)T$_2$(Py)$_B$** as a dark brown solid. $S_{BET}=373\pm10\ m^2g^{-1}$; IR (KBr): $\tilde{\nu}=3421$ (νH-bonded O-H), 2980, 2930 (νC_{sp^3}-H), 1627 (δO-H (H_2O)), 1200–1050 (νSi-O-Si), 957 (νSi-OH), 803 (δSi-OH), 458 cm^{-1} (δSi-O-Si); UV/Vis (diffuse reflectance): $\lambda_{max}=410$ nm; elemental analysis calcd (%) for $C_{49}H_{37}Cl_4CoN_7O_{90.5}Si_{43}$: C 16.44, H 1.04, N 2.74, Si 33.73, Co 1.65; found: C 14.47, H 2.42, N 2.17, Si 34.37, Co 1.71.

Preparation of the SBA-15 silica[30]

Pluronic P123 (35 g, 6.01 mmol) was dissolved in a 1.6 M aqueous solution of HCl (1.3 L). The resulting clear solution was vigorously stirred at 40 °C before tetraethoxysilane (74.37 g, 357 mmol) was added. The solution was stirred at 40 °C for 18 h. The temperature was slowly increased to reach 80 °C before stirring was stopped. After aging for three days at 80 °C, the white solid was filtered, washed thoroughly with water and methanol, and heated at 550 °C for 6 h to yield SBA-15 (20.5 g, 341 mmol, 95 %) as a fine white powder. $S_{BET}=820\pm8\ m^2g^{-1}$; IR (KBr): $\tilde{\nu}=3743$ (νH-free Si-OH), 3480 (νH-bonded O-H), 1634 (δO-H (H_2O)), 1200–1050 (νSi-O-Si), 970 (νSi-OH), 820 cm^{-1} (δSi-OH).

Post-synthesis grafting onto SBA-15

(SBA)M$_2$(Py): This material was prepared by dissolving cobalt(III) corrole **M$_2$** (110 mg, 0.12 mmol) in a suspension of SBA-15 (280 mg, 4.67 mmol) in dry toluene (15 mL) and dry pyridine (2.5 mL, 30.65 mmol, 255 equiv). The dark green mixture was stirred and heated at 80 °C for 24 h. After filtration, the solid was washed thoroughly with methanol, dichloromethane, heptane, and pentane. It was then dried under vacuum to yield **(SBA)M$_2$(Py)** (350 mg) as a dark brown powder. $S_{BET}=451\pm8\ m^2g^{-1}$; IR (KBr): $\tilde{\nu}=3427$ (νH-bonded O-H), 1631 (δO-H (H_2O)), 1200–1050 (νSi-O-Si), 958 (νSi-OH), 800 cm^{-1} (δSi-OH); UV/Vis (diffuse reflectance): $\lambda_{max}=405$ nm; elemental analysis (%) found: C 19.26, H 2.41, N 2.85, Si 32.46, Co 1.50.

(SBA)M$_2$Me(Py): This material was prepared by dissolving cobalt(III) corrole **M$_2$** (86 mg, 0.09 mmol) in a suspension of SBA-15 (210 mg, 3.5 mmol) in dry toluene (15 mL) and dry pyridine (2.5 mL, 30.65 mmol, 340 equiv). The dark green mixture was stirred and heated at 80 °C for 24 h before methyltriethoxysilane (1.46 mL, 7.28 mmol, 80 equiv) was added. The dark green mixture was stirred and heated at 80 °C for more 24 h. After filtration, the solid was washed thoroughly with methanol, dichloromethane, heptane, and pentane. It was then dried under vacuum to yield **(SBA)M$_2$Me(Py)** (284 mg) as a dark brown powder. $S_{BET}=403\pm5\ m^2g^{-1}$; ^{29}Si CP/MAS NMR (60 MHz, 25 °C, TMS): $\delta=-50.0$ (T^1), -56.4 (T^2), -65.1 (T^3), -90.9 (Q^2), -101.1 (Q^3), -110.3 ppm (Q^4); IR (KBr): $\tilde{\nu}=3423$ (νH-bonded O-H), 2976 (νC_{sp^3}-H), 1639 (δO-H (H_2O)), 1200–1050 (νSi-O-Si), 958 (νSi-OH), 800 cm^{-1} (δSi-OH); UV/Vis (diffuse reflectance): $\lambda_{max}=392$ nm; elemental analysis (%) found: C 21.20, H 2.56, N 2.73, Si 31.62, Co 1.44.

(SBA)M$_3$(Py): This material was prepared as described for **(SBA)M$_2$(Py)** from cobalt(III) corrole **M$_3$** (130 mg, 0.13 mmol), SBA-15 (313 mg, 5.21 mmol), dry toluene (15 mL) and dry pyridine (2.5 mL, 30.65 mmol, 235 equiv) to yield **(SBA)M$_3$(Py)** (420 mg) as a dark brown powder. $S_{BET}=473\pm7\ m^2g^{-1}$; IR (KBr): $\tilde{\nu}=3403$ (νH-bonded O-H), 2980, 2930 (νC_{sp^3}-H), 1633 (δO-H (H_2O)), 1558 (δN-H), 1200–1050 (νSi-O-Si), 962 (νSi-OH), 797 (δSi-OH), 457 cm^{-1} (δSi-O-Si); UV/Vis (diffuse reflec-

tance): $\lambda_{max} = 403$ nm; elemental analysis (%) found: C 14.43, H 1.58, N 2.19, Si 33.19, Co 1.57.

(SBA)M$_3$Me(Py): This material was prepared as described for **(SBA)M$_2$Me(Py)** from cobalt(III) corrole **M$_3$** (130 mg, 0.13 mmol), SBA-15 (313 mg, 5.21 mmol), methyltriethoxysilane (1.30 mL, 6.48 mmol, 50 equiv), dry toluene (15 mL) and dry pyridine (2.5 mL, 30.65 mmol, 235 equiv) to yield **(SBA)M$_3$Me(Py)** (417 mg) as a dark brown powder. $S_{BET} = 463 \pm 4\ m^2 g^{-1}$; IR (KBr): $\tilde{\nu} = 3409$ (νH-bonded O-H), 2980, 2930 (νC_{sp^3}-H), 1633 (δO-H (H_2O)), 1558 (δN-H), 1200–1050 (νSi-O-Si), 960 (νSi-OH), 798 (δSi-OH), 459 cm^{-1} (δSi-O-Si); UV/Vis (diffuse reflectance): $\lambda_{max} = 402$ nm; elemental analysis (%) found: C 15.43, H 1.89, N 2.05, Si 37.68, Co 1.58.

(SBA)D$_1$(Py): This material was prepared as described for **(SBA)M$_2$(Py)** from cobalt(III) corrole **D$_1$** (500 mg, 0.42 mmol), SBA-15 (1 g, 16.67 mmol), dry toluene (30 mL) and dry pyridine (5 mL, 61.30 mmol, 146 equiv) to yield **(SBA)D$_1$(Py)** (1.11 g) as a dark brown powder. $S_{BET} = 587 \pm 8\ m^2 g^{-1}$; IR (KBr): $\tilde{\nu} = 3436$ (νH-bonded O-H), 2232 (νC≡N), 1635 (δO-H (H_2O)), 1200–1050 (νSi-O-Si), 995 (νSi-OH), 802 cm^{-1} (δSi-OH); UV/Vis (diffuse reflectance): $\lambda_{max} = 405$ nm; elemental analysis (%) found: C 9.04, H 1.72, N 1.23, Si 38.54, Co 0.78.

(SBA)D$_1$Me(Py): This material was prepared by dissolving methyltriethoxysilane (1.12 mL, 5.59 mmol) in a suspension of **(SBA)D$_1$(Py)** (400 mg) in dry toluene (20 mL) and dry pyridine (5 mL, 65 mmol). The dark green mixture was stirred and heated at 80 °C for 24 h. After filtration, the solid was washed thoroughly with methanol, dichloromethane, heptane, and pentane, and then dried under vacuum to yield **(SBA)D$_1$Me(Py)** (402 mg) as a dark brown powder. $S_{BET} = 566 \pm 7\ m^2 g^{-1}$; IR (KBr): $\tilde{\nu} = 3400$ (νH-bonded O-H), 2232 (νC≡N), 1632 (δO-H (H_2O)), 1200–1050 (νSi-O-Si), 955 (νSi-OH), 800 cm^{-1} (δSi-OH); UV/Vis (diffuse reflectance): $\lambda_{max} = 388$ nm; elemental analysis (%) found: C 8.81, H 1.67, N 1.20, Si 37.01, Co 0.46.

Acknowledgements

This work was supported by the CNRS and Air Liquide. G.C. gratefully acknowledges the Région Bourgogne and Air Liquide for their financial support. The authors thank Mr. M. Soustelle for his assistance in the synthesis of precursors.

[1] A. W. Johnson, I. T. Kay, *Proc. Chem. Soc.* **1964**, 89.
[2] A. W. Johnson, I. T. Kay, *Proc. R. Soc. London Ser. A* **1965**, *288*, 334.
[3] A. W. Johnson, I. T. Kay, *J. Chem. Soc. A* **1965**, 1620.
[4] R. Paolesse, in *The Porphyrin Handbook, Vol. 2* (Eds.: K. M. Kadish, K. M. Smith, R. Guilard), Academic Press, New York, **2000**, pp. 201.
[5] Z. Gross, N. Galili, *Angew. Chem.* **1999**, *111*, 2536; Angew. *Chem. Int. Ed. Engl.* **1999**, *38*, 2366.
[6] Z. Gross, N. Galili, I. Saltsman, *Angew. Chem.* **1999**, *111*, 1530; *Angew. Chem. Int. Ed.* **1999**, *38*, 1427.
[7] D. T. Gryko, B. Koszarna, *Org. Biomol. Chem.* **2003**, *1*, 350.
[8] D. T. Gryko, B. Koszarna, *Synthesis* **2004**, 2205.
[9] R. Guilard, J.-M. Barbe, C. Stern, K. M. Kadish, in *The Porphyrin Handbook, Vol. 18* (Eds.: K. M. Kadish, K. M. Smith, R. Guilard), Elsevier Science (USA), **2003**, pp. 303.
[10] R. Guilard, D. T. Gryko, G. Canard, J.-M. Barbe, B. Koszarna, S. Brandès, M. Tasior, *Org. Lett.* **2002**, *4*, 4491.
[11] S. Nardis, D. Monti, R. Paolesse, *Mini-Rev. Org. Chem.* **2005**, *2*, 355.
[12] B. Koszarna, D. T. Gryko, *J. Org. Chem.* **2006**, *71*, 3707.
[13] L. Simkhovich, Z. Gross, *Tetrahedron Lett.* **2001**, *42*, 8089.
[14] G. Golubkov, J. Bendix, H. B. Gray, A. Mahammed, I. Goldberg, A. J. DiBilio, Z. Gross, *Angew. Chem.* **2001**, *113*, 2190; *Angew. Chem. Int. Ed.* **2001**, *40*, 2132.
[15] A. Mahammed, H. B. Gray, A. E. Meier Callahan, Z. Gross, *J. Am. Chem. Soc.* **2003**, *125*, 1162.
[16] I. Luobeznova, M. Raizman, I. Goldberg, Z. Gross, *Inorg. Chem.* **2006**, *45*, 386.
[17] I. Saltsman, L. Simkhovich, Y. Balazs, I. Goldberg, Z. Gross, *Inorg. Chim. Acta* **2004**, *357*, 3038.
[18] G. Golubkov, Z. Gross, *J. Am. Chem. Soc.* **2005**, *127*, 3258.
[19] J. P. Collman, M. Kaplun, R. A. Decreau, *Dalton Trans.* **2006**, 554.
[20] J.-M. Barbe, G. Canard, S. Brandès, F. Jérôme, G. Dubois, R. Guilard, *Dalton Trans.* **2004**, 1208.
[21] J.-M. Barbe, G. Canard, S. Brandès, R. Guilard, *Angew. Chem.* **2005**, *117*, 3163; *Angew. Chem. Int. Ed.* **2005**, *44*, 3103.
[22] R. J. P. Corriu, *Eur. J. Inorg. Chem.* **2001**, 1109.
[23] G. Cerveau, R. J. P. Corriu, E. Framery, *Chem. Mater.* **2001**, *13*, 3373.
[24] K. J. Shea, D. A. Loy, *Chem. Mater.* **2001**, *13*, 3306.
[25] B. Boury, R. J. P. Corriu, *Chem. Commun.* **2002**, 795.
[26] B. Boury, R. J. P. Corriu, *Chem. Rec.* **2003**, *3*, 120.
[27] J. J. E. Moreau, B. P. Pichon, M. W. Chi Man, C. Bied, H. Pritzkow, J.-L. Bantignies, P. Dieudonné, J.-L. Sauvajol, *Angew. Chem.* **2004**, *116*, 205; *Angew. Chem. Int. Ed.* **2004**, *43*, 203.
[28] A. Shimojima, Z. Liu, T. Ohsuna, O. Terasaki, K. Kuroda, *J. Am. Chem. Soc.* **2005**, *127*, 14108.
[29] J.-M. Barbe, G. Canard, S. Brandès, R. Guilard, *Eur. J. Org. Chem.* **2005**, 4601.
[30] D. Zhao, Q. Huo, J. Feng, B. F. Chmelka, G. D. Stucky, *J. Am. Chem. Soc.* **1998**, *120*, 6024.
[31] D. Y. Zhao, J. Feng, Q. Huo, N. Melosh, G. H. Fredrickson, B. F. Chmelka, G. D. Stucky, *Science* **1998**, *279*, 548.
[32] Z. Konya, J. Zhu, A. Szegedi, I. Kiricsi, P. Alivisatos, G. A. Somorjai, *Chem. Commun.* **2003**, 314.
[33] Y. Q. Wang, C. M. Yang, B. Zibrowius, B. Spliethoff, M. Linden, F. Schüth, *Chem. Mater.* **2003**, *15*, 5029.
[34] R. Richer, L. Mercier, *Chem. Mater.* **2001**, *13*, 2999.
[35] R. Guilard, C. P. Gros, F. Bolze, F. Jérôme, Z. Ou, J. Shao, J. Fischer, R. Weiss, K. M. Kadish, *Inorg. Chem.* **2001**, *40*, 4845.
[36] M. Mägi, E. Lippmaa, A. Samoson, G. Engelhardt, A.-R. Grimmer, *J. Phys. Chem.* **1984**, *88*, 1518.
[37] S. Brunauer, P. H. Emmet, E. Teller, *J. Am. Chem. Soc.* **1938**, *60*, 309.
[38] E. Barrett, L. G. Joyner, P. P. Halenda, *J. Am. Chem. Soc.* **1951**, *73*, 373.
[39] R. S. Drago, C. E. Webster, J. M. McGilvray, *J. Am. Chem. Soc.* **1998**, *120*, 538.
[40] C. E. Webster, A. Cottone, III, R. S. Drago, *J. Am. Chem. Soc.* **1999**, *121*, 12127.
[41] C. E. Webster, R. S. Drago, *Microporous Mesoporous Mater.* **1999**, *33*, 291.
[42] R. Ryoo, C. H. Ko, M. Kruk, V. Antochshuk, M. Jaroniec, *J. Phys. Chem. B* **2000**, *104*, 11465.
[43] M. Kruk, M. Jaroniec, C. H. Ko, R. Ryoo, *Chem. Mater.* **2000**, *12*, 1961.
[44] S. H. Joo, R. Ryoo, M. Kruk, M. Jaroniec, *J. Phys. Chem. B* **2002**, *106*, 4640.
[45] A. Galarneau, H. Cambon, F. Di Renzo, R. Ryoo, M. Choi, F. Fajula, *New J. Chem.* **2003**, *27*, 73.
[46] M. Jaroniec, L. A. Solovyov, *Chem. Commun.* **2006**, 2242.
[47] A. Sayari, S. Hamoudi, *Chem. Mater.* **2001**, *13*, 3151.
[48] A. P. Wight, M. E. Davis, *Chem. Rev.* **2002**, *102*, 3589.
[49] H. Yoshitake, *New J. Chem.* **2005**, *29*, 1107.
[50] F. Hoffmann, M. Cornelius, J. Morell, M. Fröba, *Angew. Chem.* **2006**, *118*, 3290; *Angew. Chem. Int. Ed.* **2006**, *45*, 3216.
[51] G. Dubois, R. Tripier, S. Brandès, F. Denat, R. Guilard, *J. Mater. Chem.* **2002**, *12*, 2255.
[52] H. Yoshitake, T. Yokoi, T. Tatsumi, *Chem. Mater.* **2002**, *14*, 4603.
[53] C. P. Jaroniec, M. Kruk, M. Jaroniec, A. Sayari, *J. Phys. Chem. B* **1998**, *102*, 5503.
[54] A. Sayari, P. Liu, M. Kruk, M. Jaroniec, *Chem. Mater.* **1997**, *9*, 2499.
[55] J.-M. Barbe, G. Canard, S. Brandès, R. Guilard, unpublished results.

Received: August 8, 2006
Published online: December 4, 2006

